Journal of Applied Physics

Direct and photon-assisted tunneling in resonant-cavity quantum-well light-emitting transistors

Cite as: J. Appl. Phys. **124**, 234501 (2018); https://doi.org/10.1063/1.5042418
Submitted: 31 May 2018 . Accepted: 20 October 2018 . Published Online: 18 December 2018

Junyi Qiu, Curtis Y. Wang, Milton Feng, and N. Holonyak

Direct and photon-assisted tunneling in resonant-cavity quantum-well light-emitting transistors

Junyi Qiu, Curtis Y. Wang, Milton Feng, and N. Holonyak, Jr.
Department of Electrical and Computer Engineering, Micro and Nanotechnology Laboratory, University of Illinois at Urbana-Champaign, Champaign, Illinois 61801, USA

(Received 31 May 2018; accepted 20 October 2018; published online 18 December 2018)

Tunneling in a transistor is a critical quantum process toward the next-generation, energy-efficient, high-speed data transfer for both electrical and optical communications. In this work, resonant-cavity quantum-well light-emitting transistors with tunneling collector junctions are designed and fabricated. Three distinctive tunneling mechanisms are clearly identified by the transistor optical output family curves, namely, electron direct tunneling (DT) from collector to base, electron DT from base to collector, and intra-cavity photon-assisted electron tunneling from base to collector. The device operations under both direct and photon-assisted tunneling are explained in detail by the intra-cavity quantum transition of electron-hole pair to photon dynamics. The tunnel junction and the corresponding carrier tunneling injection suggest the possibility of utilizing tunneling to achieve high-speed optoelectronics operations. *Published by AIP Publishing.*
https://doi.org/10.1063/1.5042418

I. INTRODUCTION

The invention of the transistor by Bardeen and Brattain[1] marks the beginning of transistor integrated circuits and serves as the basis for an information revolution. The transistor establishes the spontaneous electron-hole recombination, supporting signal amplification and switching by voltage control of the emitter and the collector junctions with minority carrier injection, recombination, and collection. Utilizing a direct bandgap compound semiconductor material, heterointerfaces, and quantum-wells (QWs), the light-emitting transistor[2,3] and the transistor laser[4,5] introduce stimulated electron-hole recombination to coherent photon generation in the base and result in a broad spectrum of new functionalities. Contrary to light-emitting diodes (LEDs) and diode lasers (DLs), where the active region is nearly intrinsic, the quantum-well transistor's base is thin and heavily doped to $10^{19}\,\mathrm{cm}^{-3}$, resulting in a short recombination lifetime and thus inherently higher optical modulation bandwidth. Experimentally, a light-emitting transistor with a modulation bandwidth $f_{-3\mathrm{dB}} = 7$ GHz corresponding to a radiative recombination lifetime of 23 ps has been reported.[6,7] Also, a transistor laser with a resonance-free 20 GHz bandwidth and a carrier recombination lifetime as low as 29 ps has been confirmed.[8] Furthermore, we have realized intra-cavity photon-assisted tunneling (ICPAT) providing the coherent photon absorption to electron-hole tunneling generation at the transistor collector junction.[9–14] This coherent-ICPAT process suggests that the collector region can be used as a built-in electro-absorption modulator (EAM) allowing direct voltage-modulation on the semiconductor laser.

Different than the previous work on coherent-ICPAT in transistor lasers,[9–16] this work focuses on the physical mechanisms of direct tunneling (DT) and incoherent-ICPAT and their interactions observed in the unique optical family characteristics of resonant-cavity light-emitting transistors (RCLETs). The new design of RCLETs includes the insertion of a double quantum-well in the base and a 15 nm $In_{0.05}Ga_{0.95}As$ layer between the base and the collector as the tunneling region. In addition to the transistor base QWs providing the electron-hole (e-h) recombination and photon generation, the collector junction incoherent-tunneling introduces additional carrier injection mechanisms and is shown to have a significant effect on the device operation; electrons tunneling from base to collector can be shown to increase the base QW photon generation because of the associated hole creation; at higher bias, ICPAT dominates and a transition from direct tunneling to inelastic tunneling is observed. Detailed DT and ICPAT tunneling mechanisms are revealed in the optical (L–V) family curves in contrast to the transistor collector current (I–V) outputs.

This work demonstrates the use of a collector tunnel junction in transistors to control emitter carrier injection, fast base transport, and QW recombination in optoelectronic devices, which may provide a much faster modulation method in comparison with the conventional current modulation of LEDs, and DLs which rely on slow diffusion for carrier supply.

II. DEVICE FABRICATION AND MEASUREMENT SETUP

The RCLET's structure and band diagram are drawn schematically in Fig. 1. The basic structure is an n-InGaP/p^+-GaAs/n^+-GaAs heterojunction bipolar transistor (HBT): the emitter is a 53 nm $In_{0.49}Ga_{0.51}P$ layer with a doping of $10^{17}\,\mathrm{cm}^{-3}$; the base region is GaAs with a doping of 10^{19}–$10^{20}\,\mathrm{cm}^{-3}$ and an undoped $In_{0.2}Ga_{0.8}As$ double QWs; the collector is GaAs with a doping of $\sim 10^{19}\,\mathrm{cm}^{-3}$; an $In_{0.05}Ga_{0.95}As$ layer of 15 nm thickness is inserted between the base and the collector to serve as the tunneling region. The resonant cavity is realized with a 4-pair distributed Bragg reflector (DBR) (12%–90% AlGaAs) on the top and a

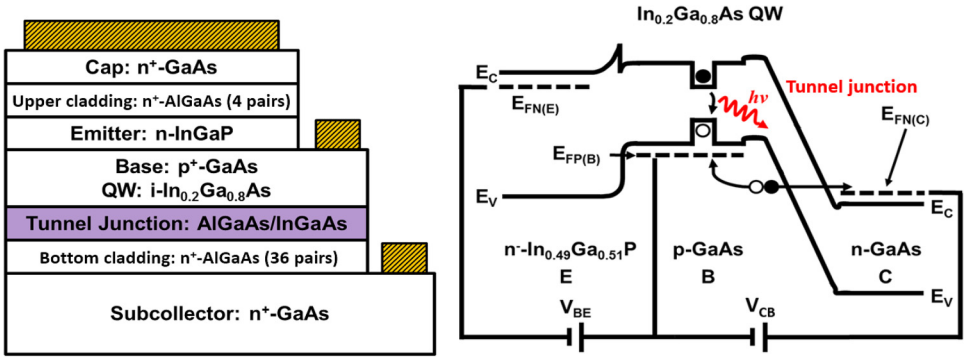

FIG. 1. Resonant-cavity quantum-well light-emitting transistor (RCLET) structure (left) and band diagram (right) showing the reduced gap tunnel junction placed at the base-collector junction and the additional hole supply due to base-to-collector electron direct tunneling under collector reverse bias.

36-pair DBR on the bottom. The device fabrication procedure can be found in previous publications.[2,3]

Figure 2 shows (a) the fabricated device under SEM and (b) the optical emission viewed with an IR camera under an optical microscope. The device has a planar contact layout for potential high-speed applications and can be probed with two sets of ground-signal-ground (GSG) probes following the conventional transistor common-emitter setup. A lensed multimode fiber (core diameter 50 μm) is used to couple the spontaneous light output from the RCLET emission area, and the spectrum is plotted in a linear scale in Fig. 2(c) with a peak wavelength at 969.8 nm and a full-width half-maximum (FWHM) of 10.6 nm. Due to the small light emission area, the lack of light output directionality, and the limited acceptance angle of fiber, we could only collect a few microwatts of power, which is a major limiting factor at this stage.

III. BASE-COLLECTOR TUNNEL DIODE I_{BC}–V_{BC} CHARACTERISTICS

The diode I_{BC}–V_{BC} characteristics of the base-collector (BC) junction are measured at room temperature to confirm the existence of tunneling behavior. As shown in Fig. 3(a), a negative differential resistance region appears in the diode I–V curve, which is the signature of a tunnel diode.[14] The device band diagram is simulated with Sentaurus TCAD and plotted in Fig. 3(b) for reference. When the collector junction is reverse biased ($V_{BC} < 0$ V), electrons tunnel from the base valence band to the collector conduction band; at a small BC junction forward bias ($V_{BC} > 0$ V), electrons tunnel from the collector conduction band to the base valence band; under higher forward bias ($V_{BC} > 0$ V), electrons diffuse from the collector to the base. The C-to-B tunnel current increases with the junction bias until the collector Fermi-level aligns with the base valence band, at which point a peak current (I_P) of 2.35 mA is recorded at a peak voltage (V_P) of 0.14 V; further increasing the junction bias will reduce the amount of available equal-energy states in the base valence band and reduce the tunnel current, giving rise to the negative differential resistance. The simulated band diagram shows that the separation between the base valence band and the collector Fermi-level is 0.074 eV, which is smaller than the measured peak voltage; this is likely due to the non-negligible series resistance introduced by contact resistance and the device

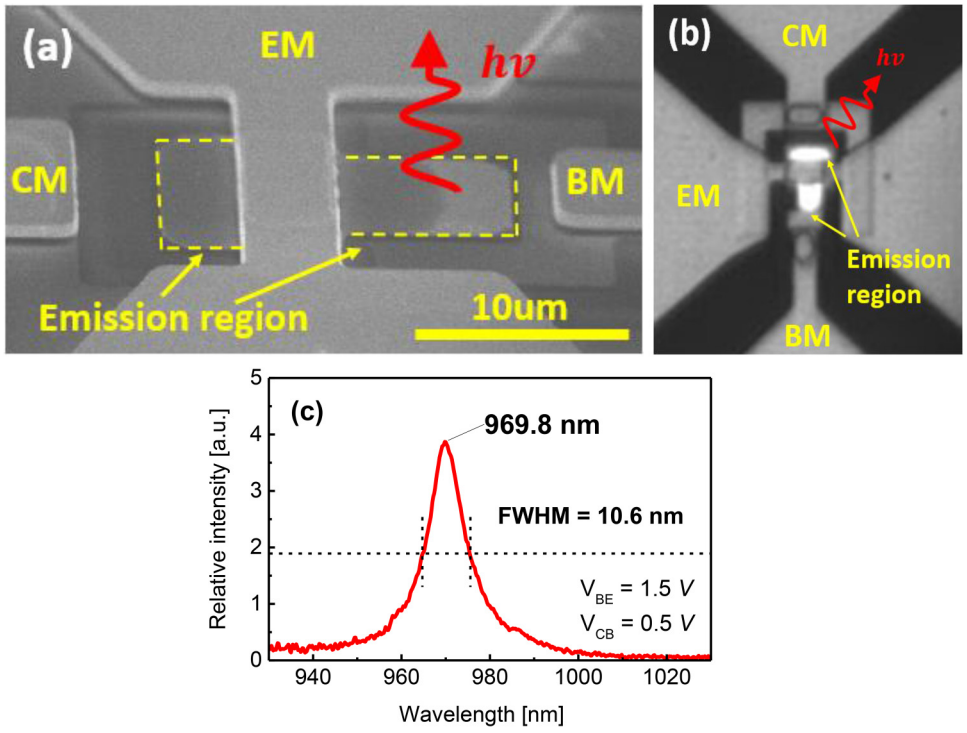

FIG. 2. (a) SEM image of the finished RCLET device; the contacts are placed on the top with emitter metal (EM), base metal (BM), and collector metal (CM). (b) Microscopic top view of the device under testing; light emission (~980 nm) can be observed with an IR camera; a lensed multimode fiber is used to couple the light output; only a fraction of the total power can be collected due to the small emission area and the lack of light output directionality. (c) RCLET emission spectrum measured at a bias of $V_{BE} = 1.5$ V and $V_{CB} = 0.5$ V; the peak emission is at 969.8 nm with a full-width half-maximum of 10.6 nm.

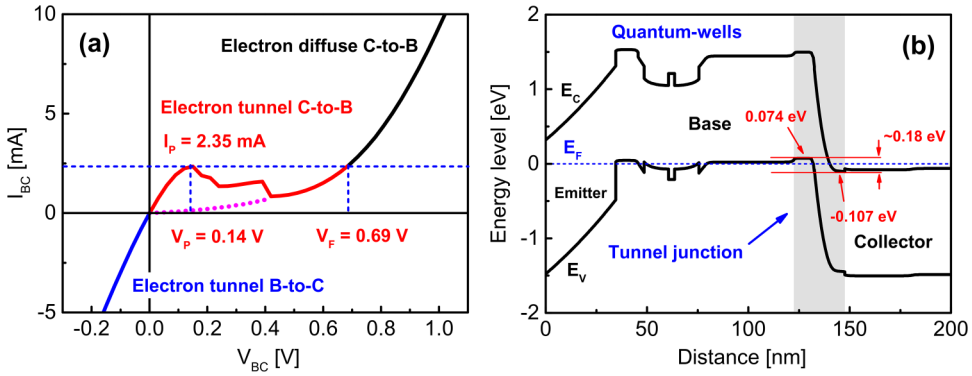

FIG. 3. (a) Room-temperature base-collector junction tunnel diode *I–V* measurement showing the negative differential resistance region (red) as a result of direct tunneling, which is consistent with the behavior of tunnel diodes.[14] The emitter-base voltage is kept at zero (shorted) during the measurement. The current and voltage polarities are chosen in accordance with the tunnel diode convention. A peak current of 2.35 mA is recorded at a peak voltage of 0.14 V; the forward voltage is 0.69 V; the valley current and voltage cannot be easily determined due to the fluctuations in the negative differential region; the purple dotted line shows the fitting of the exponential diode *I–V* curve. (b) RCLET band diagram simulation done with Sentaurus TCAD to show the energy level alignment in the base-collector tunnel junction; at equilibrium, the base valence band edge is estimated to be 0.074 eV above the Fermi-level, and the collector conduction band edge is 0.107 eV below the Fermi-level. However, the measured peak voltage V_P in Fig. 3(a) is twice the expected value (the simulated potential difference between the base valence band and the collector Fermi-level), probably due to the non-negligible series resistance introduced by the contact resistance and extrinsic region.

extrinsic region. Note that the fluctuations in the negative differential resistance region are due to the oscillation caused by the measurement instrument's control loop, and thus we were not able to obtain a smooth curve to accurately determine the valley current and voltage.

IV. TRANSISTOR ELECTRICAL I_C–V_{CB} AND OPTICAL L–V_{CB} FAMILY CURVES

The BC diode characteristics in Fig. 3(a) are redrawn with inverted current-voltage polarities as shown in Fig. 4(i) for easy comparison to the RCLET collector current outputs. The transistor base current I_B, collector I_C–V_{CB}, and the corresponding optical L–V_{CB} family of curves are measured and plotted in Figs. 4(ii)–4(iv). Different from the typical common-emitter bipolar transistor's collector output I_C–V_{CE} family curves, i.e., sweeping V_{CE} at constant I_B levels, the RCLET is characterized by sweeping V_{CB} at constant V_{BE} levels in order to reveal clearly the voltage-controlled BC junction tunneling output behavior. Figures 4(ii)–4(iv) illustrate the transistor operation with the collector junction bias going from forward ($-1 < V_{CB} < 0$ V) to reverse ($0 < V_{CB} < 3$ V) and the emitter junction under forward bias ($0 < V_{BE} < 2$ V, $\Delta V_{BE} = 0.25$ V).

Four different transistor operation regions are shown in Fig. 4(iii) collector I_C–V_{CB} and 4(iv) optical L–V_{CB}. Specifically, one diffusion and three tunneling mechanisms are identified: (A) electron diffusion from collector to base and hole diffusion from base to collector under collector junction strong forward bias; (B) direct electron tunneling from collector to base under weak forward bias; (C) direct electron tunneling from base to collector under weak reverse bias; and (D) intra-cavity photon-assisted electron tunneling from base to collector under strong reverse bias; the detailed analysis and explanations can be found in Sec. V, with the band diagram schematics, carrier distribution, recombination, and transport corresponding to the different operating regions (A, B, C, and D) plotted in Figs. 5–8 to explain the device behaviors.

The simulated band diagram in Fig. 3(b) suggests that the transistor already pinches-off at zero BC junction bias; thus, the RCLET is fully functional at $V_{CB} = 0$ V. In Fig. 4(ii), when the BE junction is not turned on yet ($0 < V_{BE} < 1$ V), the base current plot is exactly the same as the BC diode curve because all the carrier movements in the base come from the BC junction, and $I_B = 0$ when $V_{CB} = 0$; when the BE junction turns on with $V_{BE} > 1$ V, the base sees an additional electron injection from the BE junction; thus, the base recombination will increase, causing the base to draw more positive charges from the base terminal and the base current increases regardless of V_{CB} bias, and $I_B > 0$ when $V_{CB} = 0$. In Fig. 4(iv), when the BC junction is forward biased at $V_{CB} < 0$ V, holes will leak from the transistor base to collector and thus reduce the QW photon generation, which is reflected in the optical L–V_{CB} family curves by the reduced optical output power in both regions A and B compared with when $V_{CB} = 0$ V. However, when the BC junction is reverse biased at $V_{CB} > 0$ V and we allow electrons to tunnel from base to collector, the optical output starts to increase despite the constant base hole supply; at the extreme case when $V_{BE} = 0$ V, i.e., zero base hole supply, there is still light output except at a higher V_{CB} bias. This phenomenon is explained in Sec. V and can be attributed to the hole (empty states) creation in the base due to electrons tunneling from the base valence band to the collector conduction band, and thus region C represents the tunneling carrier injection supplying the photon generation process, which is a novel approach in contrast to the conventional carrier diffusion supply, and has the benefit of fast modulation speed (limited by femtosecond tunneling time) and high sensitivity (exponential tunneling *I–V* relation). For example, as shown in Fig. 4(iv) L–V_{CB} family curves, it is possible to bias the device at $V_{BE} = 1.75$ V and modulate V_{CB} between 0 and 1 V to realize an efficient, direct-voltage, tunneling modulation on the optical output in addition to the conventional base current injection modulation.

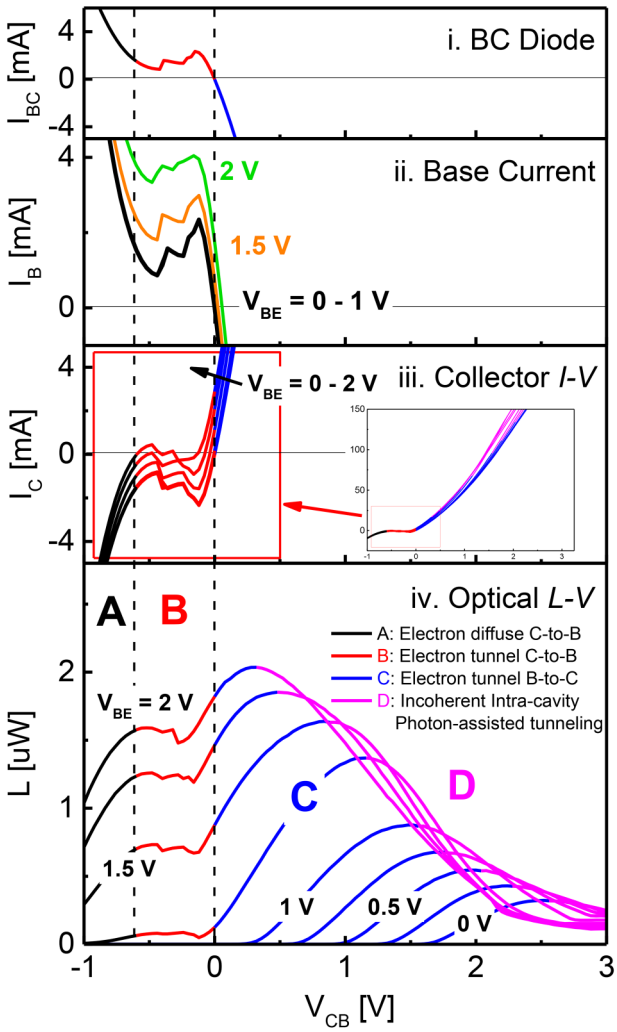

FIG. 4. RCLET electrical and optical family curves measured with V_{CB} from –1 to 3 V and V_{BE} from 0 to 2 V. The base current (ii) follows the BC tunnel diode curve (i) when $V_{BE} < 1$ V and is offset by the emitter-to-base injection when $V_{BE} > 1$ V. The collector current (iii) increases exponentially in the high bias region due to BC junction tunneling. The negative slope when $-0.5 < V_{CB} < 0$ V corresponds to the negative differential resistance region of the BC tunnel diode. Four operating regions (A–D) can be identified that correspond to different diffusion or tunneling mechanisms. Four band diagrams are drawn schematically in Figs. 5–8, respectively. The optical power is measured by fiber coupling with a lensed multimode fiber, thus the low coupling efficiency.

Currently, due to RCLET's spontaneous emission and fiber coupling setup, the received optical power level is too low for meaningful RF characterization; additionally, the fact that the fiber could only couple a fraction of the total light output means we cannot quantitatively analyze the RCLET's internal electron-photon conversion rate or quantum efficiency. In the future, we may redesign the device layout to improve the light output directionality and extraction efficiency in order to obtain a high signal-to-noise ratio for modulation experiments.

V. ANALYSIS ON OPTICAL L–V_{CB} TUNNELING OPERATION REGIONS

Figure 5 shows that the transistor base-collector junction is under forward bias with $-1 < V_{CB} < 0$ V and the emitter

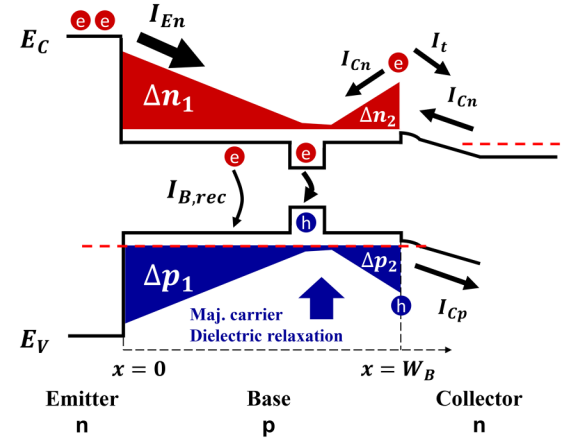

FIG. 5. Band diagram corresponding to region (A) in the transistor family curves in Fig. 4 for the transistor collector junction under forward bias with $-1 < V_{CB} < -0.5$ V and the emitter junction also under forward bias with $0 < V_{BE} < 2$ V ($\Delta V_{BE} = 0.25$ V). In this case, the collector Fermi-level is above the base valence band. In region (A), the collector current I_C is a forward diffusion current due to the lower collector barrier confinement. Minority electrons from both the emitter (Δn_1) and the collector (Δn_2) diffuse into the base region. The majority holes (Δp_1) and (Δp_2) originate from the dielectric relaxation from the base contact in response to the minority electron injection to maintain the base charge neutrality.

junction is also under forward bias with $0 < V_{BE} < 2$ V ($\Delta V_{BE} = 0.25$ V), as in region (A). The minority carrier distributions in the base (Δn_1) and (Δn_2) are diffused from both the emitter and the collector, respectively; the majority carrier (hole) distributions (Δp_1) and (Δp_2) are responding to the minority carrier electron injection via dielectric relaxation from the base contact to maintain the base charge neutrality. Thus, the collector current (I_C) is equal to the sum of the collector-to-base electron diffusion current (I_{Cn}) and the base-to-collector hole diffusion current (I_{Cp}), both of which are in the opposite direction of the collector current defined under the normal transistor forward active operation, and I_{Cp}

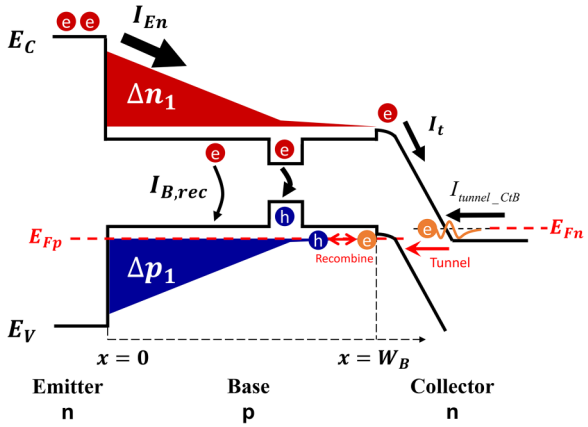

FIG. 6. Band diagram corresponding to region (B) in the family curves in Fig. 4 for the transistor collector junction under forward bias with $-0.5 < V_{CB} < 0$ V and the emitter junction also under forward bias with $0 < V_{BE} < 2$ V ($\Delta V_{BE} = 0.25$ V). In this case, the collector Fermi-level is between the base valence-band and the base Fermi-level. Electrons tunnel from collector to base and recombine with base holes, reducing the QW radiative recombination and light output. The tunnel current is in the opposite direction of the collector current and results in the collector current reduction $I_C = I_t - I_{tunnel\_CtB}$ or the negative differential resistance.

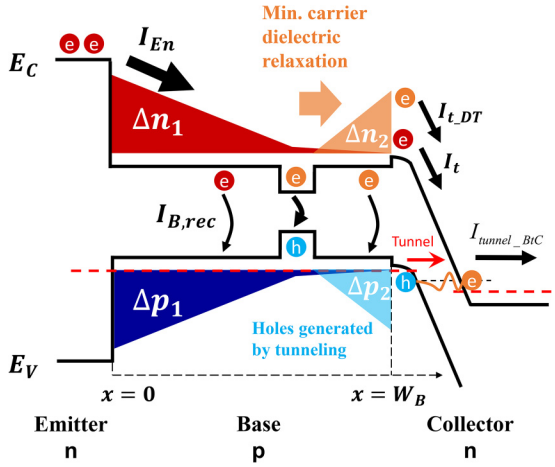

FIG. 7. Band diagram corresponding to region (C) in the family curves in Fig. 4 for the transistor collector under reverse bias with $0 < V_{CB} < 3$ V and the emitter under forward bias with $0 < V_{BE} < 2$ V ($\Delta V_{BE} = 0.25$ V). In this case, the collector Fermi-level is below the base Fermi-level. Electrons tunnel from base to collector, creating additional holes in the base and thus increasing the light output. The tunnel current is in the same direction as the collector current. The base holes (Δp_2) are created by electron direct tunneling from base to collector; this causes the electron accumulation (Δn_2) in the conduction band near the collector junction which increases the collector drift current (I_{t_DT}). Thus, $I_C = I_t + I_{t\_DT} + I_{tunnel\_BtC}$ and a DT current gain can be defined as $\beta_{DT} = (I_{t\_DT} + I_{tunnel\_BtC})/I_{tunnel\_BtC}$.

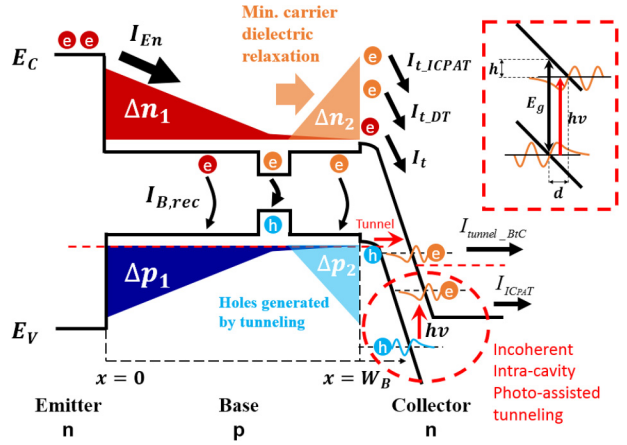

FIG. 8. Band diagram corresponding to region (D) in the family curves in Fig. 4 for the collector under reverse bias with $0 < V_{CB} < 3$ V and the emitter-base junction under forward bias with $0 < V_{BE} < 2$ V ($\Delta V_{BE} = 0.25$ V). In this case, the collector Fermi-level is further below the base Fermi-level. Electrons are direct tunneling from base to collector as well as intra-cavity photon-assisted tunneling (ICPAT) from base to collector. The maximum of optical output is reached when the photon generation rate by e-h recombination at the QWs is equal to the photon absorption rate by ICPAT at the collector. When the photon generation rate is less than the photon absorption rate, the light output is reduced. Two tunnel currents exist and are both in the same direction as the collector current. Thus, $I_C = I_t + I_{t\_DT} + I_{t\_ICPAT} + I_{tunnel\_BtC} + I_{ICPAT}$ and a new tunneling (DT + ICPAT) current gain can be defined as $\beta_{ICPAT} = (I_{t\_DT} + I_{t\_ICPAT} + I_{tunnel\_BtC} + I_{ICPAT}) / (I_{tunnel\_BtC} + I_{ICPAT})$.

can be regarded as the hole leakage from the base region. Finally, the base current (I_B) as seen from the terminal is equal to the base recombination current ($I_{B,rec}$) plus I_{Cp} with a positive current direction, because positive charges need to be injected into the base from the terminal in order to balance the hole reduction through recombination ($I_{B,rec}$) and leakage (I_{Cp}), which is indicated in Fig. 4(ii). Note that the optical output (L) is proportional to the base recombination current $I_{B,rec}$, and we denote the overall conversion efficiency as η. When the collector junction forward bias decreases, the hole leakage current I_{Cp} is reduced; thus, both I_C and the optical output will increase but I_B will decrease as shown in the transistor I_C–V_{CB} and L–V_{CB} family curves. We may express the transistor electrical and optical outputs in region (A) as

$$I_C = I_t - I_{Cn} - I_{Cp} = \alpha I_{En} - I_{Cn} - I_{Cp}, \tag{1}$$

$$L = \eta I_{B,rec} = \eta(I_B - I_{Cp}), \tag{2}$$

where α denotes the base transport factor and I_{En} is the emitter-to-base electron injection current.

When the collector junction voltage V_{CB} places the collector Fermi-level (E_{Fn}) between the base valence band (E_V) and the base Fermi-level (E_{Fp}), the collector electrons tunnel to the empty states in the base, as shown in Fig. 6. This results in a direct tunneling current I_{tunnel_CtB} in the opposite direction of I_C. Since the electrons tunneling to the base will occupy the empty states in the valence band and effectively recombine with holes, the base terminal current I_B will increase in response as shown in the negative differential region in Fig. 4(ii); and since it is a non-radiative process which leave fewer holes available for radiative recombination, both the collector current and the optical output reduce [the negative differential resistance region in Figs. 4(iii) and 4(iv)]. We express the electrical and optical outputs in region (B) as

$$I_C = I_{t1} - I_{tunnel\_CtB}, \tag{3}$$

$$L = \eta I_{B,rec} = \eta(I_B - I_{tunnel\_CtB}). \tag{4}$$

When V_{CB} approaches zero (equilibrium), I_{tunnel_CtB} will decrease due to the lack of available empty states at the base side; thus, both I_C and optical outputs reach minimum and recover, resulting in the negative slope region (B).

When the collector Fermi-level (E_{Fn}) is below the base Fermi-level (E_{Fp}) under collector reverse bias, the base valence band electrons tunnel to the empty states above the collector Fermi-level as shown in Fig. 7. This direct tunneling current (I_{tunnel_BtC}) increases I_C and creates additional holes (Δp_2, states empty of electrons), which then drift toward the QWs for radiative recombination; therefore, the base recombination current ($I_{B,rec}$) and the light output will increase [Fig. 4(iv)]; meanwhile, the base current I_B as seen by the terminal will decrease and even become negative because the base now can have an excess of positive charges due to the hole creation by collector tunneling [Fig. 4(ii)]. The excess positive charges in the base will also lower the emitter-base junction energy barrier and allow the electrons (negative charge) to be injected from the emitter via dielectric relaxation transport in order to maintain charge neutrality in the base region. Thus, the corresponding electrons (Δn_2) will accumulate near the collector junction and result in the additional collector drift current I_{t_DT} and provide (base + QWs) recombination. Thus, the typical transistor diffusion current gain β can be obtained and a new

direct tunneling (DT) current gain β_{DT} can be defined. We may write for region (C)

$$I_C = I_t + I_{t\_DT} + I_{tunnel\_BtC}, \tag{5}$$

$$L = \eta I_{B,rec} = \eta(I_B + I_{tunnel\_BtC}), \tag{6}$$

$$\beta = \frac{I_t}{I_B} \quad \text{and} \quad \beta_{DT} = \frac{I_{t\_DT} + I_{tunnel\_BtC}}{I_{tunnel\_BtC}}. \tag{7}$$

For $V_{BE} = 0$, the emitter diffusion current $I_t = 0$ and only base-to-collector direct tunnel (DT) electrons can occur at $V_{CB} \geq 0$ as shown in the collector I_C–V_{CB} relation. However, the holes (Δp_2) will take a longer time to diffuse to the QWs for radiative recombination compared with the short response time of the base dielectric relaxation electron transport and the collector drifting. Thus, the additional DT collector drift current I_{t_DT} contributes significantly to the total collector current T_C owing to the large tunneling current gain. Hence, we need to raise $V_{CB} \geq 1.5$ V to obtain more DT electrons in order to achieve steady-state light output as shown in Fig. 4(iv) region (C) on the $V_{BE} = 0$ trace. Since the diffusing current $I_t = \alpha I_{En}$ and I_B increases with increase in V_{BE}, the light output (L) increases with increasing DT and base current I_B.

Figure 8 shows that the base electrons tunnel to the collector via both DT and incoherent intra-cavity photon-assisted tunneling (ICPAT) under higher collector reverse bias. As the DT current increases with V_{CB} and the base current I_B increases with V_{BE}, the base QW radiative recombination (photon generation) rate will increase as shown in Fig. 4(iv) region (C). The cavity photon confinement by the top and bottom DBR structures and the strong electric field in the collector junction provides the necessary conditions for photon-assisted tunneling for photon absorption and e-h generation. Since the photon absorption rate at the collector junction by ICPAT (governed by the tunneling time) is faster than the photon generation rate in the base QWs (limited by the recombination lifetime), the light output reaches a maximum and then decreases. The collector current output does not easily separate between the e-h generation from DT and ICPAT; however, the optical output clearly exhibits the distinct difference as shown in Fig. 4(iv) region (C) for DT and region (D) for ICPAT. We may write for region (D)

$$I_C = I_t + I_{t\_DT} + I_{t\_ICPAT} + I_{tunnel\_BtC} + I_{ICPAT}, \tag{8}$$

$$\begin{aligned} L &= \eta I_{B,rec} - L_{absorb} \\ &= \eta(I_B + I_{tunnel\_BtC} + I_{ICPAT}) - L_{absorb}, \end{aligned} \tag{9}$$

$$\beta_{ICPAT} = \frac{I_{t\_DT} + I_{t\_ICPAT} + I_{tunnel\_BtC} + I_{ICPAT}}{I_{tunnel\_BtC} + I_{ICPAT}}, \tag{10}$$

where I_{ICPAT} accounts for the electron current swept to the collector terminal due to ICPAT, I_{t_ICPAT} accounts for the dielectric relaxation transport current in response to ICPAT, and L_{absorb} accounts for the photon absorption due to the same effect, and we again define a new tunneling gain β_{ICPAT} that accounts for both DT and ICPAT. Thus, we demonstrate in the L–V_{CB} family curves (Fig. 4) three tunneling processes: collector-to-base electron direct tunneling, base-to-collector electron direct tunneling, and base-to-collector electron intra-cavity photon-assisted tunneling, all of which are controlled by V_{CB}.

VI. CONCLUSION AND FUTURE WORKS

Resonant-cavity quantum-well light-emitting transistors with tunneling collector junctions are designed, fabricated, and analyzed. Unique transistor electrical and optical behaviors are observed as a result of the carrier DT and ICPAT tunneling. By sweeping the base-collector junction bias, the switching between three tunneling mechanisms is clearly observed. Thus, the introduction of a tunneling collector has significantly modified the optical output of a light-emitting transistor. These results support the possibility of applying tunneling modulation on optoelectronic devices and utilizing the ultrafast tunneling process to achieve high-speed operations.

ACKNOWLEDGMENTS

The authors wish to acknowledge the support of Dr. Michael Gerhold of the Army Research Office (ARO) under Grant No. W911NF-17-1-0112. They also would like to acknowledge the Pao Family fellowship. This project has been partially supported by the National Science Foundation under Grant No. 1640196 and the Nanoelectronics Research Corporation (NERC), a wholly-owned subsidiary of the Semiconductor Research Corporation (SRC), through Electronic-Photonic Integration Using the Transistor Laser for Energy-Efficient Computing, an SRC-NRI Nanoelectronics Research Initiative under Research Task ID 2697.001. They appreciate Mr. Adam B. Auten for the low temperature setup and measurement on the tunneling junction measurement.

[1]J. Bardeen and W. H. Brattain, Phys. Rev. **74**, 230 (1948).
[2]M. Feng, N. Holonyak, Jr., and W. Hafez, Appl. Phys. Lett. **84**, 151 (2004).
[3]M. Feng, N. Holonyak, Jr., and R. Chan, Appl. Phys. Lett. **84**, 1952 (2004).
[4]G. Walter, N. Holonyak, Jr., M. Feng, and R. Chan, Appl. Phys. Lett. **85**, 4768 (2004).
[5]M. Feng, N. Holonyak, Jr., G. Walter, and R. Chan, Appl. Phys. Lett. **87**, 131103 (2005).
[6]C. H. Wu, H. W. Then, M. Feng, N. Holonyak, Jr., and G. Walter, Appl. Phys. Lett. **94**, 171101 (2009).
[7]G. Walter, C. H. Wu, H. W. Then, M. Feng, and N. Holonyak, Jr., Appl. Phys. Lett. **94**, 231125 (2009).
[8]M. Feng, H. W. Then, N. Holonyak, Jr., G. Walter, and A. James, Appl. Phys. Lett. **95**, 033509 (2009).
[9]A. James, J. Holonyak, Jr., M. Feng, and G. Walter, IEEE Photonics Technol. Lett. **19**, 680 (2007).
[10]M. K. Wu, M. Feng, and N. Holonyak, Jr., Appl. Phys. Lett. **101**, 081102 (2012).
[11]M. Feng, J. Qiu, C. Y. Wang, and N. Holonyak, Jr., J. Appl. Phys. **119**, 84502 (2016).
[12]M. Feng, J. Qiu, C. Y. Wang, and N. Holonyak, Jr., J. Appl. Phys. **120**, 204501 (2016).
[13]C. H. Wu and C. H. Wu, in *CS MANTECH Proceedings* (CS MANTECH Conference, 2014), p. 87.
[14]L. Esaki, Phys. Rev. **109**, 603 (1958).
[15]G. E. Stillman and C. M. Wolfe, "Avalanche photodiodes," in *Infrared Detector (II), Semiconductors and Semimetals* (Academic Press, 1977), Vol. 12, pp. 291–391.
[16]C. M. Wolfe, N. Holonyak, Jr., and G. E. Stillman, *Physical Properties of Semiconductors* (Prentice Hall, Englewood Cliffs, NJ, 1989), pp. 219–220.